JAAS

Accepted Manuscript

This is an Accepted Manuscript, which has been through the Royal Society of Chemistry peer review process and has been accepted for publication.

Accepted Manuscripts are published online shortly after acceptance, before technical editing, formatting and proof reading. Using this free service, authors can make their results available to the community, in citable form, before we publish the edited article. We will replace this Accepted Manuscript with the edited and formatted Advance Article as soon as it is available.

You can find more information about Accepted Manuscripts in the author guidelines.

Please note that technical editing may introduce minor changes to the text and/or graphics, which may alter content. The journal's standard Terms & Conditions and the ethical guidelines, outlined in our author and reviewer resource centre, still apply. In no event shall the Royal Society of Chemistry be held responsible for any errors or omissions in this Accepted Manuscript or any consequences arising from the use of any information it contains.

ROYAL SOCIETY OF CHEMISTRY

rsc.li/jaas

FPM model calculation for micro X-ray fluorescence confocal imaging using synchrotron radiation

I. Szalóki[1], A. Gerényi[1], G. Radócz[1], A. Lovas[1], B. De Samber[2] and L. Vincze[2]

[1] Institute of Nuclear Techniques, Budapest University of Technology and Economics

[2] Department of Analytical Chemistry, Ghent University, 9000 Ghent, Belgium

A novel quantitative reconstruction model for synchrotron based confocal X-ray fluorescence imaging has been developed and validated. The theoretical approach uses new generalized system of equations of the Fundamental Parameter Method (FPM) to calculate the 2D distribution of the concentration values of the trace, minor and major elements. For the reconstruction procedure of the 2D quantitative μXRF calculations a serial-type specialised iterative algorithm was developed based on successive approximation of the elementary composition of each individual voxel in the sample. This procedure is capable of neglecting serious numerical difficulty arising at the simultaneous approaching solution of the huge number of variables involved in the non-linear FPM equations. The model describes the absorption of the primary and secondary X-ray beams in the sample volume and the photoelectric excitation process of characteristic X-ray emission in each sample voxel. For validation of this new evaluation method, standard samples were measured using monoenergetic synchrotron radiation at Beamline L in HASYLAB.

Introduction

Since the nineties various kind of X-ray lenses have been developed and applied for micro XRF spectroscopy which optical devices are appropriate for focusing X-ray beam and provide a significantly increased photon flux at the sample surface comparing to conventional X-ray measuring set-up, where only a pinhole is used forming X-ray beam. The lateral resolution can be achieved by using polycapillary X-ray lenses down to 10 μm in the focal spot that property offers an excellent

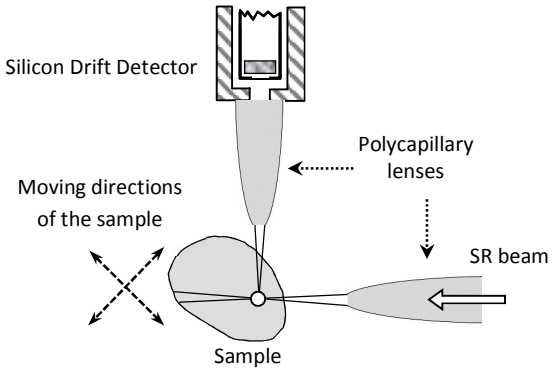

Figure 1. Confocal measuring set-up for X-ray fluorescence imaging performed by SR beam.

applicability of this device in micro-X-ray fluorescence analysis (μXRF) using confocal geometrical set-up. In conventional X-ray fluorescence measurements, the information provided by the emitted photons originates from the whole length of beam-path in the sample volume, therefore the depth-resolved distribution of the elementary concentrations cannot be determined. In confocal set-up two polycapillary X-ray lenses are used in μXRF experimental arrangement: one half-lens is mounted in front of the detector and the other one is set between the sample and the X-ray source. The focal spots of these optical units have to be adjusted into the same voxel in the sample[1]. The primary X-ray beam propagates through the first polycapillary lens that optics transmits it into a convergent X-ray beam towards the focal spot of the X-ray lens. The sample is set into a certain position: an optional inner point of the sample is set into the common focal spot of the confocal measuring set-up and in this position the EDXRF spectra can be recorded. Mostly those photons are detected which are emitted from the sample volume determined by the focal spot. A part of photons emitted from outer parts of the focal volume can contribute to the detected signal as well; however in this study we neglect this effect. This measuring method provides a volume-selective determination of 2D or 3D elementary maps of the sample. One of the major advantages of application of polycapillary optics is the elimination of significant part of scattered X-ray radiation emitted by the outside region of the focal volume of the optical set, which geometrical condition improves the detection limit[2]. Typical measuring sketch of a simple confocal set-up is introduced on Figure 1.. This technical arrangement provides an excellent possibility for depth-dependent quantitative X-ray fluorescence analysis. Since 1990, owing to the rapid improvement in synchrotron

measuring technology and X-ray focusing devices μXRF technique has become one of the most significant non-destructive procedures for determination of 2D or 3D distribution of chemical elements in few-mm-sized objects.

The quantification of the combination of FPM and confocal technique requires the knowledge of the measuring properties of the capillary optics. One of the attributions of capillary lenses is the energy dependent transmission which optical property changes the intensity-distribution of the X-ray beam. Therefore, applying confocal measuring mode in synchrotron based μXRF or μXANES experiments the transmission function of the capillary lens versus energy has to be known[3]. One of the possibilities to estimate the transmission function of the applied polycapillary lens is the Monte Carlo simulation. The authors of publication [4] calculated the excitation spectrum of a microfocus tube and the transmission function that was obtained by Monte-Carlo simulation carried out by MCNP4C code. Empirical method was applied for determination of the transmission function of X-ray lens by the measurement of two scattered spectra, with and without lens[5]. The other important property of the polycapillary lenses is the shape and intensity distribution of the excitation spectra. The real form of the intensity distribution at cross section of the focal spot can be approximated by Gaussian function for each direction of coordinates[6]. However, this approximation causes mathematical difficulties in both theoretical and numerical calculations.

One of the key problems of confocal techniques is the quantification. Smith at. al.[7] developed a new analytic model for the quantitative depth-analysis of paint layers of historical objects. This model describes the absorption of X-rays in the outer layers and calculates the secondary fluorescence contribution induced by the neighbouring layers. Quantitative determination of polymer layers was performed by Schaumann et. al.[8] using 3D confocal set-up. The low-Z matrix allows the calculation of thickness of the layers without interference of matrix effect. Woll and his co-workers[9] used combination of polycapillary collector and single-bounce monocapillary optics at synchrotron beam in confocal set-up and they developed a semi-empirical model for calculation the geometrical parameters of a layered paint structure on surface of glass samples. Application of a new iterative solution based on FPM approach was developed by Perez at. al.[10] for samples having layered structure, in order to analyse composition and thickness of intermediate layers. The authors of publication [11] reported a deterministic-type mathematical model which exactly describes the secondary fluorescence enhancement effect in confocal measuring set-up. Due to the rather complicated mathematical formalism, they proposed a numerical solution using minimization algorithms for producing the concentrations. FPM based quantitative model was extended to confocal setup for μXRF with application of X-ray optics for 3D elementary analysis[12]. This validated calibration model and calculation procedure provided a possibility for determination of the transmission function of the applied polycapillary lens used in detection channel. This calibration mode is based on the measurement of fluorescence signal of thin standard samples, and it provides the simultaneous determination of X-ray tube spectrum and transmission of the X-ray optic. For portable X-ray spectrometers a new calibration method[13] was developed, used for analysis of layered samples, which procedure can be applied for confocal set-up as well. For application of confocal measuring geometry high photon flux is required, therefore this technique is usually used at synchrotron beamlines, but recently some new applications for laboratory systems were published as well[14]. Combination of metal ceramic-type microfocus X-ray tube with a full polycapillary and a half lens in front of the SD detector provides useful practical table-top confocal depth-selective μXRF device[15]. This type of confocal set-up is suitable for constructing a transportable version of this type of device[16] using half lenses for detection and microfocus X-ray tube. Confocal set-up for table-top XRF system was built for 3D microanalysis on paintings, metal and glass surfaces, glazes and inclusions in gemstones[17]. The detection limit for this simple and cost-effective XRF equipment is significantly less than it can be achieved at synchrotron beams, about 2 orders of magnitude, however for preliminary experiments this new analytical construction seems to be very promising.

Due to the combination of intense synchrotron beam and confocal μXRF set-up results a very efficient and flexible analytical tool allowing investigation of 3D elementary composition of wide variation of different type of samples, especially of objects of cultural heritage. Kanngießer at. al.[18] reported one of the first applications of confocal μXRF studies on investigation of cultural heritage objects with synchrotron radiation achieving 10 μm depth resolution which size allowed of distinguishing different paint layers by means of depth-dependent elementary compositions. Application of confocal μXRF method for analysis of historical glass objects was reported in publication[19] where the authors studied the applicability of this technique by both synchrotron radiation and X-ray tube by analysis of painted layers on glasses. Famous historical examinations by confocal X-ray fluorescence imaging was published on a hidden painting[20] of Vincent van Gogh analysing a relatively large area of the paintings (17.5 × 17.5 cm^2) by a 0.5x0.5 mm monochromatic SR beam. By determination of the elementary distribution (Mn, Cr, Co, Fe, Cu, Zn, As, and Ba) in different paintings layered on each other they could discover the hidden painting.

One of the most dynamically developed part of this measuring field is the biological applications where the elementary maps of major and trace elements in selected parts of plants or animals are measured. The biological samples generally contain relatively high amount of light elements, which property could result the evaporation of the organic compounds during excitation by a brilliant synchrotron beam. This effect should cause the damage of water-rich microstructures of the irradiated tissues and individual cells. In order to neglect this non-preferable effect cryogenic conditions have to be applied during the measuring period. Application of liquid nitrogen steam[21] (T≈78 K) is an ideal and efficient solution for this measuring problem, however the low-temperature stream is dangerous for the capillary optics,

namely it can be broken due to the strong thermal stress. Practical health reasons motivated the application of confocal μXRF for determination the contamination and accumulation of As, Cd, Cu, Mn, Ni and Ti elements in single rice grains[22]. Confocal XRF measuring set-up at synchrotron beam was applied in 3D investigation of biological model organism Daphnia magna[23] for mapping tissue-specific distribution of Zn, Ca and Fe. For determination of the quantitative maps of these elements the distribution of density function of the samples were measured by a laboratory CT system equipped with microfocus X-ray tube.

Special application field of confocal technique is the geo- and planetary science. A new measuring technique was developed for analysis of cometary dust samples[24] fixed in aerogel holder. For the data analysis new solution of data evaluation was developed based on the combination of confocal method with FPM and PCA analysis in ESRF at beamline ID13. After mathematical comparison of the FPM equations describing the excitation of elements in a grain-like sample and in an appropriately selected standard reference material the weight fractions were calculated by numerical iterative algorithm. Geoscience application was published by Brenker et. al.[25] measuring the composition of mineral inclusions in diamonds those probably were originated from lower mantle of the Earth for elements in range of atomic number $20 < Z < 92$. Finally, some overview on measuring properties of this technique was published. K. Janssens and his co-workers[26] published introducing the confocal μXRF measuring technique, its applications in field of environmental studies, cultural heritage, nuclear and earth sciences. Another overview on X-ray polycapillary optics was presented in[27] including history of these optical devices, theory of working principle, modelling of focusing effect and it demonstrates the wide applicability within wide variety of measuring geometries for table top and SR spectrometers.

FPM model for confocal μXRF imaging

The ultimate goal of the confocal-type μXRF measurements is to determine 2D or 3D maps of elementary composition in optionally selected plane or in sub-volume of the investigated sample, i. e. to determine the quantitative composition of each voxel. Due to the unknown attenuation of the matrix, serious experimental and calculation difficulties occur in empirical calibration of such kind of μXRF confocal measurement where the matrix has heterogeneous composition. Therefore, standardless and quantitative determination using FPM[28] based mathematical description of the excitation and the attenuation effect in the sample material offers a reasonable solution for determination of the 2D or 3D elementary maps. Applying the general FPM procedure, the elementary compositions in each sample voxel around the actual location of focal spot of the confocal geometrical set-up can be determined.

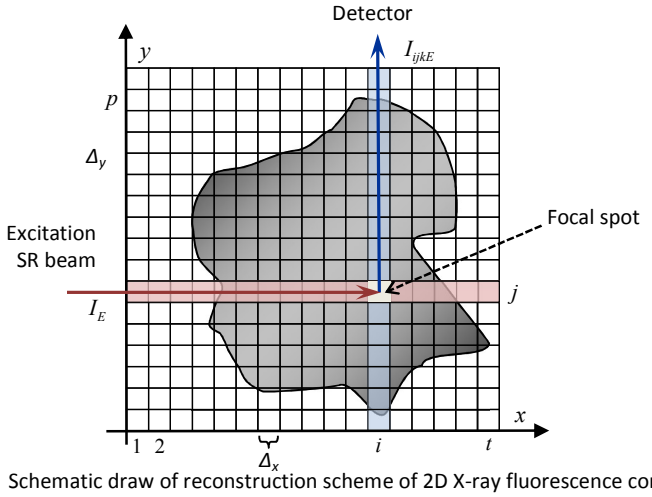

Figure 2. Schematic draw of reconstruction scheme of 2D X-ray fluorescence confocal imaging.

This proposed model calculation requires the knowledge of the attenuation of the sample material in each voxel along the paths of both primary and secondary X-ray beams. Figure 2. introduces the reconstruction scheme for FPM calculation algorithm with indication of the primary and secondary X-ray beams. In order to simplify the rather complex FPM calculation procedure we supposed a parallel shape with homogeneous distribution of the flux density of X-ray photons in the excitation X-ray beam in section perpendicular to the direction of the beam propagation. The sample mass in each voxel are supposed to be homogeneous. Assume this section of the sample is involved in a rectangle shape dividing into $p \cdot t$ pieces of individual voxels with $V = \Delta_x \Delta_y \Delta_z$ volume of each. Generally, the size of the focal spot of polycapillary optics[29,27] depends on the energy of the X-ray beam and the voxel size as function of the energy can be approximated [30] as given by the first term of (1). For further calculations, we suppose that both primary and secondary capillaries have the same optical parameters. Corresponding to relations (1) the minimum value of the voxel sizes is Δ. The area of the cross-section of the primary beam is $\Delta_y \Delta_z = \Delta\Delta$ corresponding to its energy E (see Figure 3.), but the size of the focal spot as x coordinate is determined by the detector polycapillary that varies corresponding to the energy of the characteristic radiations. In relations

(1) variable E is the energy of the excitation beam and Δ_k is the voxel size at energy of the characteristic radiation (used for FPM calculation) of the k^{th} element of the sample ($1 \le k \le n$) where the n is the number of chemical elements in the sample.

$$\Delta \sim \frac{1}{E} \Rightarrow \Delta_k = \Delta \frac{E}{E_k} \quad \text{if} \quad E_k \le E \Rightarrow \Delta \le \Delta_k$$
$$\Delta \le \Delta_k = \Delta_x \qquad \Delta_y = \Delta \qquad \Delta_z = \Delta \qquad k = 1,\ldots,n \tag{1}$$

Corresponding to (1) the volume of each individual voxel is $V = \Delta_k \Delta\Delta$. In this model, the size of the voxels and the step size of translations of the sample during the confocal measurements are defined to be equal to the size of the primary beam (Δ) that value must be determined experimentally. The beam sizes can be approximated as FWHM[31] of Gaussian shape of the intensity distribution. However, in order to simplify the mathematical description the recent model does not take into account the real intensity distribution of the beams; it is substituted by a constant value. Calculating the focal volume on the basis of the step size, the nearby voxels overlap each other; however this influence on the calculated weight fractions of the elements is neglected.

The primary X-ray beam enters into the sample volume at voxel (1,*j*) and some photons propagate into direction of voxel (*i*,*j*). The intensity of the primary beam decreases due to the absorption of the excitation channel, namely in set of voxels involved in the j^{th} row from voxel (1,*j*) toward to voxel (*i*-1,*j*). Before entering the primary beam into voxel (*i*,*j*) the flux density I^*_{jE} (number of photons per unit area per second) can be calculated by equation (2).

$$I^*_{jE} = I_E \exp\left(-\Delta \sum_{s=1}^{i-1} \sum_{m=1}^{n} \rho_{sj} C_{sjm} \mu_{mE}\right) \qquad C_{sjm} = \begin{cases} \ge 0 \text{ in voxel} = (s,j) \\ = 0 \text{ in voxel} \ne (s,j) \end{cases} \quad m = 1,\ldots,n \tag{2}$$

In system of equations (2) the parameter I_E is the photon flux density of the mono-energetic excitation X-ray beam with energy E before entering into the sample matrix. The ρ_{sj} is the mass density of the sample in the voxel (s,j). Variable μ_{mE} is the attenuation coefficients of the m^{th} element at photon energy *E*.

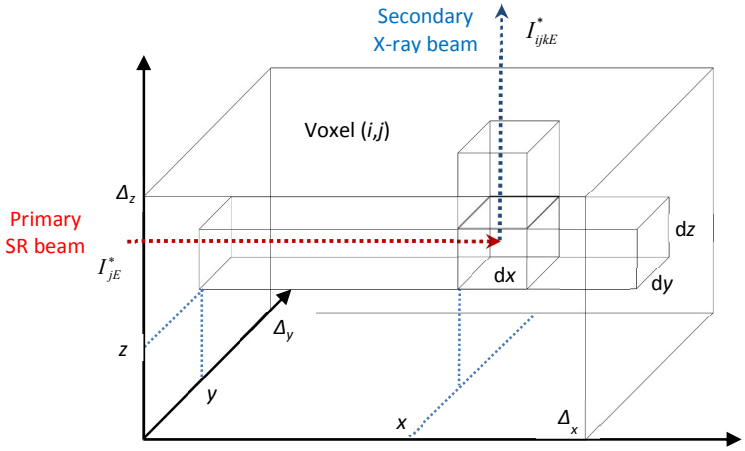

Figure 3. Calculation of the absorption correction factor A_{ijkE} for voxel (*I*,*j*).

Supposed that each voxel has individual elementary composition; therefore, the attenuation property varies voxel-by-voxel. The variable C_{sjm} is the weight fraction (or concentrations) of the m^{th} element in voxel (s,j). The chemical elements in voxel (i,j) emit X-ray fluorescence radiations with photon flux I^*_{ijkE}.

The integral equations (3) can be written as non-linear relationships between weight fractions of chemical elements C_{ijk} and the flux of emitted characteristic radiations I^*_{ijkE} at the top border of the voxel (i,j) (see. Figure 3). Some emitted photons propagate into the direction of the detector that is considered by the solid angle of the detector (Ω).

$$I^*_{ijkE} = \frac{\Omega}{4\pi} \rho_{ij} g_{kE} C_{ijk} I^*_{jE} \int_0^{\Delta_z} \int_0^{\Delta_y} \int_0^{\Delta_x} \exp\left(-x\rho_{ij} \sum_{m=1}^{n} C_{ijm} \mu_{mE}\right) \exp\left(-z\rho_{ij} \sum_{m=1}^{n} C_{ijm} \mu_{mk}\right) dx dy dz = \frac{\Omega}{4\pi} \rho_{ij} g_{kE} C_{ijk} I^*_{jE} A_{ijkE} \quad k = 1,\ldots,n \tag{3}$$

The expression $g_{kE} = \omega_k R_k K_k \mu_{kE}$ is the fluorescence excitation function of the k^{th} element, which formula consists of multiplication of photoelectric cross section (substituting by mass photo-absorption function μ_{kE}) for the k^{th} element, radiative rate (R_k), fluorescence yield (ω_k) of the k^{th} element and the absorption jump ratio (K_k) [28]. Taking into consideration relations (1) the integrals (3) can be calculated and a new variable A_{ijkE} (4) can be defined as the absorption correction factor for the k^{th} element's characteristic radiation in voxel (i,j).

$$A_{ijkE} = \Delta \frac{1-\exp\left(-\Delta_k \rho_{ij} \sum_{m=1}^{n} C_{ijm}\mu_{mE}\right)}{\rho_{ij}\sum_{m=1}^{n} C_{ijm}\mu_{mE}} \frac{1-\exp\left(-\Delta \rho_{ij} \sum_{m=1}^{n} C_{ijm}\mu_{mk}\right)}{\rho_{ij}\sum_{m=1}^{n} C_{ijm}\mu_{mk}} \quad (4)$$

This formula contains the attenuation effect for both primary and secondary radiations in voxel (i,j). Some characteristic X-ray photons propagate from voxel (i,j) toward the detector in the column (i) and leave the sample volume at voxel (i,p). The variable μ_{mk} is the absorption parameter of the m^{th} element for the characteristic radiation of the k^{th} element. Let us introduce by equations (5) a new variable as I_{ijkE} referring as detected characteristic X-ray flux emitted by the k^{th} element (k=1,…,n) those are involved in voxel (i,j). The last exp-type part in the system (5) describes the attenuation of the characteristic X-ray radiations in the detection channel between voxels (i,j+1) and (i,p).

$$I_{ijkE} = \frac{\Omega}{4\pi}\varepsilon_k \eta_k T_k \rho_{ij} g_{kE} C_{ijk} A_{ijkE} I_E \exp\left(-\Delta \sum_{m=1}^{n}\left(\sum_{s=1}^{i-1}\rho_{sj} C_{sjm}\mu_{mE} + \sum_{r=j+1}^{p}\rho_{ir} C_{irm}\mu_{mk}\right)\right), \quad (5)$$
$$i = 1,\ldots,t \qquad j = 1,\ldots,p \qquad k = 1,\ldots,n$$

In equations (5) Ω is determined by the actual geometrical arrangement that parameter depends mostly on the sample-detector distance and the area of the detector surface. The function T_k represents the transmission function of the acceptance capillary half-lens at energy of the characteristic radiation of the k^{th} element. The absorption of the air layer between sample and detector window is η_k that given by functions (6). The μ_{airk} represents the attenuation parameter of the air at energy of characteristic radiation of the k^{th} element and d_{air} is the thickness of the air layer32. The first expression (ε_k) in (6) approximates the detection efficiency versus energy.

$$\begin{aligned} \varepsilon_K &= \exp\left(-\mu_{Bek} d_{Be}\rho_{Be} - \mu_{Sik} d_{ia}\rho_{Si}\right)\left(1-\exp\left(-\mu_{Sik} d_{ac}\rho_{Si}\right)\right). \\ \eta_k &= \exp\left(-\mu_{airk} d_{air}\rho_{air}\right) \end{aligned} \quad (6)$$

The variables μ_{Bek}, μ_{Sik} are the absorption coefficients of different detector layers located between the sample and the detector crystal, d_{Be}, d_{ia}, d_{ac} are the thicknesses and ρ_{Be}, ρ_{Si} are the mass densities of these layers[32]. For the calculation of the unknown values of the weight fractions in voxel (i,j) the system of equations (7) can be expressed by derivation from set of equations (5). These equations are not independent from each other because they contain C_{ijm} as implicit variables as well. In (7) the variable F_E is the instrumental factor defined as the reciprocal multiplication of two constant parameters: density of the photon flux of the primary X-ray beam and the acceptance solid angle of the detector. Variables D_k involves both the transmission of the acceptance capillary and the absorption of the air along the beam-paths into the detector direction (outside of the sample volume) at energy of characteristic line of the k^{th} element. This term contains also the full energy efficiency function of the detector at the same energy.

$$C_{ijk} = \underbrace{\frac{4\pi}{\Omega\, I_E}}_{\tilde{F}_E} \underbrace{\frac{1}{\varepsilon_k \eta_k T_k}}_{\tilde{D}_k} \underbrace{\frac{I_{ijkE}}{\rho_{ij} g_{kE} A_{ijkE}}}_{\tilde{G}_{ijkE}} \underbrace{\exp\left(\Delta \sum_{m=1}^{n}\left(\sum_{s=1}^{i-1}\rho_{sj} C_{sjm}\mu_{mE} + \sum_{r=j+1}^{p}\rho_{ir} C_{irm}\mu_{mk}\right)\right)}_{\tilde{M}_{ijkE}} \quad (7)$$
$$i = 1,\ldots,t \qquad j = 1,\ldots,p \qquad k = 1,\ldots,n$$

The weight fractions of the chemical elements are not included in terms F_E and D_k. The variables G_{ijkE} and M_{ijkE} involve the C_{ijm}, but they are mathematically independent from each other, because they contain such weight fractions those are belonging to two disjoint groups of voxels.

(i) The variables G_{ijkE} express the absorption effect influencing on calculated concentration of the k^{th} element in voxel (i,j), i.e. the G_{ijkE} variables depend on that C_{ijm} (m=1, …,n) those variables are belonging only to voxel (i,j).

(ii) The fourth term in equations (7) symbolized by M_{ijkE} depends on the absorption properties of linear set of voxels where the primary beam propagates from voxel (1,j) to (i-1,j) before entering into voxel (i,j). After excitation in voxel (i,j) a part of secondary X-ray beam spreads from voxel (i,j+1) to (i,p) towards the detector. This separability condition in equations (7) for variables C_{ijk} indicates that terms G_{ijkE} and M_{ijkE} are mathematically independent from each other.

Therefore, the property (ii) allows constructing an appropriate algorithm of numerical calculation of a simple solution of the system of equations (7) avoiding the necessity of simultaneously numerical solution of this system of equations.

Algorithm for solution of confocal FPM equations

The number of equations in system (7) is equal to $t{\cdot}p{\cdot}n$ and the number of unknown variables should arrange 2-5·10^4 in a simple case of μXRF confocal imaging measurement. Consequently, the huge number of equations generates serious numerical processing difficulty if the simultaneous solution is applied. However, the separability property of the system of equations (7) offers a simple algorithm for calculation of the weight fractions that avoids this numerical problem. If the composition of those voxels, which voxels influence (trough the absorption) the excitation and detected X-ray fluxes is

known the numerical solution becomes much simpler. Due to the algebraically separated structure of equations (7) it allows organizing an appropriate order for the numerical solution of the system of equation (7) in each voxel corresponding to the following algorithm.

(i) The numerical procedure starts in the first voxel of row which located closest to the detector and closest to the X-ray source (1,p) (see Figure 2.). The series of steps of calculations is continued following the propagation direction of excitation X-ray beam, therefore the second calculation step is done in the neighbour voxel (2,p) and it proceeds step-by-step following the sequence seen below

$$(1,p) \rightarrow (2,p) \rightarrow \ldots \rightarrow (t\text{-}1,p) \rightarrow (t,p).$$

(ii) After completing the calculation in the first row (1,p) → (t,p) a new series of calculation starts from left to right direction in the second row

$$(1,p\text{-}1) \rightarrow (2,p\text{-}1) \rightarrow \ldots \rightarrow (t\text{-}1,p\text{-}1) \rightarrow (t,p\text{-}1).$$

Applying this sequence in the serial of numerical calculation, it allows determining the quantitative composition of each individual voxel. If the compositions of all voxels which influence the results of calculation through their absorption in the actual voxel have been determined before the calculation in voxel (i,j) is performed, the composition of voxel (i,j) can be determined exactly. Due to the non-linear and implicit nature of equations (8) (derived from (7)), a successive approximation algorithm is required to solve numerically for all possible combination of index *i, j, k*.

$$C_{ijk} = F_E D_k M_{ijkE} \frac{I_{ijkE}}{\rho_{ij} g_{kE}} \frac{1}{A_{ijkE}} \quad i = 1,\ldots,p \quad j = 1,\ldots,t \quad k = 1,\ldots,n \tag{8}$$

In system (8) variables A_{ijkE} depend on the unknown weight fractions of chemical elements (C_{ijm} m=1, …,n) in voxel (i,j). Other variables as F_E, D_k do not contain any C_{ijm}. The terms involved in variables M_{ijkE} must be determined in previous steps of the algorithm. The remaining mathematical problem is to search the numerical solution of equations (8) in voxel (i,j) for each element (k=$1,\ldots,n$). In publication[28] we presented an own developed and tested algorithm for simple numerical approximation in order to determine the value of weight fractions involved in the non-linear system of equations of the FPM problem. This procedure is based on a separate measurement of characteristic intensities of chemical elements in standard reference material (SRM) or pure chemical elements.

Transmission of capillary lens

The above theoretical algorithm requires experimental determination of variables T_k and F_E as input functions for the numerical calculations. These two terms can be calculated by an independent XRF measurement on an extremely thin (1-5 ng/mm^2) SRM that allows to neglect the matrix effect. In the case of a very thin sample, two variables involved in equations (8) approach to constant values as it introduced by (9).

$$\Delta, \Delta_k << 1 \quad \Rightarrow \quad A_{ijkE} \approx \Delta^2 \Delta_k \qquad M_{ijkE} \approx 1 \tag{9}$$

In order to determine the energy dependence for the transmission efficiency function (T_p) of the acceptance polycapillary lens a new formula (10) can be derived from equations (7) and (9)

$$T_p = \frac{4\pi I_{pE}}{\Omega\, I_E \varepsilon_p \eta_p g_{pE} C_p \rho \Delta^2 \Delta_p} \sim \frac{I_{pE}}{\varepsilon_p \eta_p g_{pE} m_p} \qquad m_p = \rho C_p \Delta^3 \quad p = 1,\ldots,q \tag{10}$$

where m_p is the mass per unit area (gram per cm^2) for the p^{th} element and I_{pE} is the number of characteristic X-ray photons (per second per unit area) of the p^{th} element emitted from the irradiated part of the thin SRM sample. Due to the extremely low thickness of the SRM layer, the irradiated area is $\Delta\Delta < \Delta_p\Delta_p$ therefore in equation (10) Δ can be used instead of Δ_{p}. The variable q is the number of chemical elements and ρ is the density of the SRM sample. In expressions (10) the absorption effect in the excited area is disregarded due to the low thickness (≈ 200 nm) of the layer. The definitions of other variables in equations (10) are equivalent to the similar parameters defined in the previous section. For the determination of the I_{pE} function, the following parameters referred by the test report of the polycapillary focusing optic was applied: transmission at 17 keV was given as T_p(E=17 keV)≈1.1% . We have calculated the values of transmission at individual energies using equations (10) and fit an empirical function[5] described by equation (11)

$$T_E = aE^b \exp(-cE), \tag{11}$$

where E is the energy of the secondary X-ray radiation entering into the acceptance capillary . In order to determine the unknown instrumental factor F_E in equations (8), a standard reference sample was measured under the same geometrical and excitation conditions as were applied for the measurement of the real sample. The result of the determination of the transmission of polycapillary lens is shown on Figure 4.

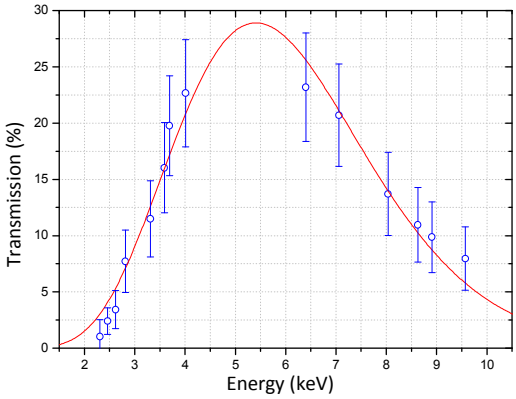

Figure 4. Transmission of the polycapillary lens in detector channel versus energy.

Due to the multi-element composition of this SRM sample, the instrumental factor was determined at different X-ray energies corresponding to the characteristic energy of the k^{th} elements in the SRM (F_{kE}) . The relationship between F_{kE} and other parameters such as concentration values (C_k) of chemical elements in the standard reference sample, physical properties of the excitation beam and the detection efficiency is derived from equation (10)

$$F_{kE} = \frac{T_{kE} \Delta_0 g_{kE} C_k \varepsilon_k \eta_k A_{kE}}{I_k} \qquad k = 1,\ldots,w \tag{12}$$

where w is the number of chemical elements in the standard sample used for determination of F_{kE}. The selected voxel for XRF measurement performed for determination of F_{kE} was located in the first column and in the first row in that side of sample where the excitation beam entered the sample body.

Dark matrix

The semiconductor-type detectors used for X-ray measurements are mostly equipped with Be window having thickness in the range of 8-25 µm, which parameter limits the detectable elements for atomic numbers (13<Z). Therefore one portion of the sample elements are undetectable, those part consists of low-Z elements, however applying polymer based thin-window for the X-ray detector the 'visible' atomic range may be expanded down to Z=6. According to this fact the sample elements may be classified into two main groups depending on their atomic number.

(i) The first group of the sample elements (indexed by i=1,…,d) consists of low-Z elements, those are undetectable. Concerning the un-detectability of these low-Z elements the matrix which involves these elements is defined as "dark matrix"[33].

(ii) The characteristic X-ray lines of the second group of elements (indexed by i=d+1,…,n) are detectable, i.e. the atomic numbers of these elements can be identified on the basis of their X-ray fluorescence radiation and their concentration can be calculated.

General solution of the dark matrix problem using FPM based approaches has been not exactly completed yet, only different approximations have been developed to estimate the absorption functions of the dark matrix[34]. For simplification of the currently applied FPM model, let us introduce the effective atomic number (Z_{ijD}) of the dark matrix in voxel (i,j) defined by equation (12). W_k is the atomic weight of the k^{th} element in the dark matrix. This definition offers a possibility to approximate the energy dependent absorption function of the dark matrix. The effective atomic number belongs to a virtual chemical element that substitutes the completely undetectable dark matrix as absorber medium. This definition means that the multi-element dark matrix is characterised by a single virtual chemical element in the FPM equations[35, 36].

$$\left.\begin{array}{l} Z_1,\ldots,Z_d,Z_{d+1},\ldots,Z_n \\ C_{ij1},\ldots,C_{ijd},C_{ijd+1},\ldots,C_{ijn} \end{array}\right\} \Rightarrow Z_{ijD} = \frac{\sum_{k=1}^{d} W_k C_{ijk} Z_k}{\sum_{k=1}^{d} W_k C_{ijk}} = Z_D \tag{12}$$

Note, in this point we supposed, that the dark matrix has exactly the same composition in each individual voxel in the sample. Only the value of the weight fraction of the complete dark matrix should change voxel by voxel, therefore the set of {Z_{ijD}} can be substituted by a single number Z_D. Values of the absorption coefficients can be estimated versus energy by empirical relationship $\mu_{DE} = a_1 Z_D^{a_2}$ [30, 36]. Equations (13) give the calculation mode of the sample attenuations (μ_{ijE} and μ_{ijk}) in voxel (i,j). The variables μ_{Dk} ,μ_{DE} are the absorption of the dark matrix in voxel (i,j) at energy of the k^{th} element characteristic radiation and the excitation energy, respectively.

$$\mu_{ijE} = C_D \mu_{DE} + \sum_{m=d+1}^{n} C_{ijm} \mu_{mE} \quad \mu_{ijk} = C_D \mu_{Dk} + \sum_{m=d+1}^{n} C_{ijm} \mu_{mk}$$
$$C_D = 1 - \sum_{m=d+1}^{n} C_{ijm} \tag{13}$$

If the effective atomic number of the dark matrix cannot be approximated, one can determine it experimentally by measurement of the elastic and inelastic scattering of the excitation beam in the sample matrix and by calculation their intensity ratio. In case of light matrix, the other way should be the precognition of the quantity of the main components of the sample matrix as the dark matrix. For example, at the case of biological samples, the major elements in the matrix composition does not change drastically voxel by voxel therefore the average chemical composition can be estimated. If the normalisation condition is valid (see the last equation in (13)), the parameter C_D can be eliminated by normalization of the current values of the weight fractions in each iteration step in each voxel. In order to perform the above detailed numerical calculations we constructed a new software in MatLab environment. The numerical procedure for calculation of fundamental atomic data (absorption functions, excitation parameters) was applied as it is published in [30]. The energy dependent focal size Δ_k (see eq. (1)) is involved implicitly in equation of the absorption correction factor given by eq. (4). This function was not available, therefore for avoiding of the lack of these unknown variables the absorption factor was determined by a relative measurement on the same SRM sample which was used for the test of the calculation model.

$$C_{ijkE}^{(s)} = C_{ijkE}^{(r)} \frac{I_{ijkE}^{(s)} \rho_{ij}^{(r)} A_{ijkE}^{(r)}}{I_{ijkE}^{(r)} \rho_{ij}^{(s)} A_{ijkE}^{(s)}} \exp\left(\Delta \sum_{m=1}^{n} \left(\sum_{s=1}^{i-1} \rho_{sj}^{(s)} C_{sjm}^{(s)} \mu_{mE} + \sum_{r=j+1}^{p} \rho_{ir}^{(s)} C_{irm}^{(s)} \mu_{mk} \right) \right) \tag{14}$$
$$i = 1,\ldots,t \qquad j = 1,\ldots,p \qquad k = 1,\ldots,n$$

For the depth dependent determination of the concentrations in studied NIST SRM sample (details see below in the next chapter) an additional measurement was performed on that voxel which was closest to the X-ray source and the detector. In this case the primary and the secondary absorption caused by the sample mass in other voxels was neglected. In equations (14) the depth dependent calculation of concentrations signed by (s) is done by comparison on the result of this reference measurement signed by (r).

$$C_{ijkE}^{(s)} = C_{ijkE}^{(r)} \frac{I_{ijkE}^{(s)}}{I_{ijkE}^{(r)}} \exp\left(\Delta \sum_{m=1}^{n} \left(\sum_{s=1}^{i-1} \rho_{sj}^{(s)} C_{sjm}^{(s)} \mu_{mE} + \sum_{r=j+1}^{p} \rho_{ir}^{(s)} C_{irm}^{(s)} \mu_{mk} \right) \right) \tag{15}$$
$$i = 1,\ldots,t \qquad j = 1,\ldots,p \qquad k = 1,\ldots,n$$

The system of equations (15) describes the final calculation of the sample concentrations that is free from energy dependent voxel size, and both the density and the self-absorption coefficients of the sample were supposed to be constant in the whole sample volume.

Experiments and results

X-ray fluorescence confocal imaging based on synchrotron radiation was assembled and performed for the determination of 2D/3D distributions of elemental composition in small (1-2 mm) sized samples at HASYLAB Beamline L. For validation of the numerical procedure detailed in previous sections, confocal micro-XRF analyses on NIST SRM 1577c standard reference materials were carried out. The excitation energy of the monochromatic SR beam was fixed at energy of E=21keV and 17 keV using Ni/C multilayer monochromator. The polycapillary X-ray lens used as detector acceptance was produced by XOS, which had input focal distance 2.2 mm and the transmission at energy of 17 keV for source diameter less than 10 µm was 1.1 %.

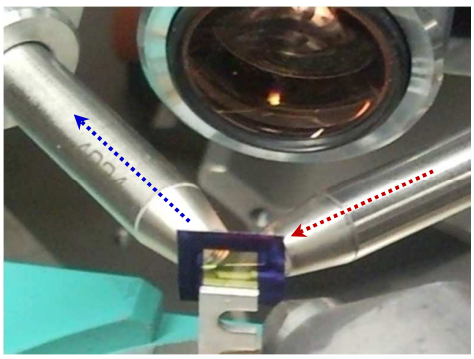

Figure 5. Measuring set-up for the film-type reference sample.

The lateral resolution achieved was between 10 and 20 µm during the measurement of the elemental maps in biological samples. Therefore, the average beam size in the focal volume was set around 15 µm that value determined the step-size of the scanning procedure. In order to determine the transmission of capillary lens in the detector channel thin standard reference material (TSRM) was measured under exactly the same geometrical and excitation conditions as it was applied for the sample measurement (see Figure 5.). Film-type reference sample (RF4-200-S1749-6 produced by AXO Dresden GmbH) was used, that special sample was developed for confocal experiments performed by narrow synchrotron beam. The material of TSRM was deposited on silicon nitride film having 200 nm thickness and the sample material contained Pb, La, Pd, Mo, Cu, Fe and Ca elements in the range of 1-20 ng/mm^2. Deviation of the lateral homogeneity on the sample material was less than 1% for each element. The certified composition of the sample is involved in Table 1.

Element	Pb	La	Pd	Mo	Cu	Fe	Ca
Mass (ng/mm^2)	7.61	11.01	1.8	1.32	2.84	5.04	19.31
Deviation of the sample mass (ng/mm^2)	0.96	0.62	1.0	0.4	0.35	0.87	1.1

Table 1. Composition of the RF4-200-S1749-6 standard sample.

The fitted transmission function of acceptance polycapillary lens versus X-ray energy with the fitted curve given in equation (11) and the result is plotted on Figure 4. in the previous chapter. For confocal test measurements NIST SRM 1577c (Bovine liver) was used in pressed pellet form and mounted on xyz moving stage at HASYLAB Beamline L.

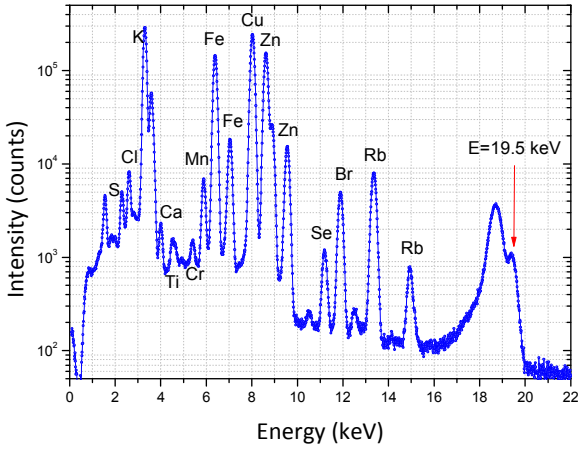

Figure 6. XRF sum spectra for determination of the evaluation parameters for MICROXRF2 software.

The measuring time of each individual voxel was set as 10 s, therefore the time requirement of the whole analysis was around 7-10 hours. The XRF spectra were evaluated by nonlinear least-squares fitting software MICROXRF2 package designed for automatic deconvolution of huge number of ED-XRF spectra. The core of this software package involved the validated numerical routines of AXIL[37] software. The MICROXRF2 code was designed for complete evaluation of the XRF spectra as deconvolution of peaks, elimination of escape peaks and sum peaks as well. In order to get confocal XRF images each individual XRF signal were normalized to 100 mA SR current. Due to the rather poor statistics in each spectrum recorded from different voxels the numerical evaluation model-parameters were determined by the sum of all the spectra (Figure 5.) measured during the whole confocal scan on the same sample. In order to test and validate the theoretical FPM calculations in confocal mode using monochromatic excitation synchrotron beam, series of measurements on two standard reference material samples were carried out: NIST SRM 1577c (Bovine liver)[38] and NIST SRM 611 (glass standard)[39]. The measuring set-up used for these measurements was similar to the case of film-type reference sample. Both SRM samples were mounted on aluminium holder frame. The monochromatized SR beam was focused by XOS-type polycapillary lens onto the flat surface of the sample close to the edge.

Figures 7.-9. show the result of the measurement for the intensity distribution of the Kα radiations of different chemical elements involved in the samples. At the case of the SRM 1577c deeper part of the sample material was irradiated and excited due to the considerably lower absorption comparing to the SRM 611 glass sample. The maps on the right side of these colour plots show the distribution of the FPM calculated concentration of the chemical elements. The intensity distributions of the characteristic intensities are inhomogeneous, but the calculated concentrations form a rather homogeneous picture on the excited part of the sample demonstrating the effectiveness of the theoretical confocal model. Statistical fluctuation can be recognised on the calculated maps of the concentrations due to the local inhomogeneity of the

physical properties of the sample material such as density. In deeper part of the sample the flux of the primary SR beam decreases due to the attenuation of the sample material, therefore the uncertainty of the beam intensity increases.

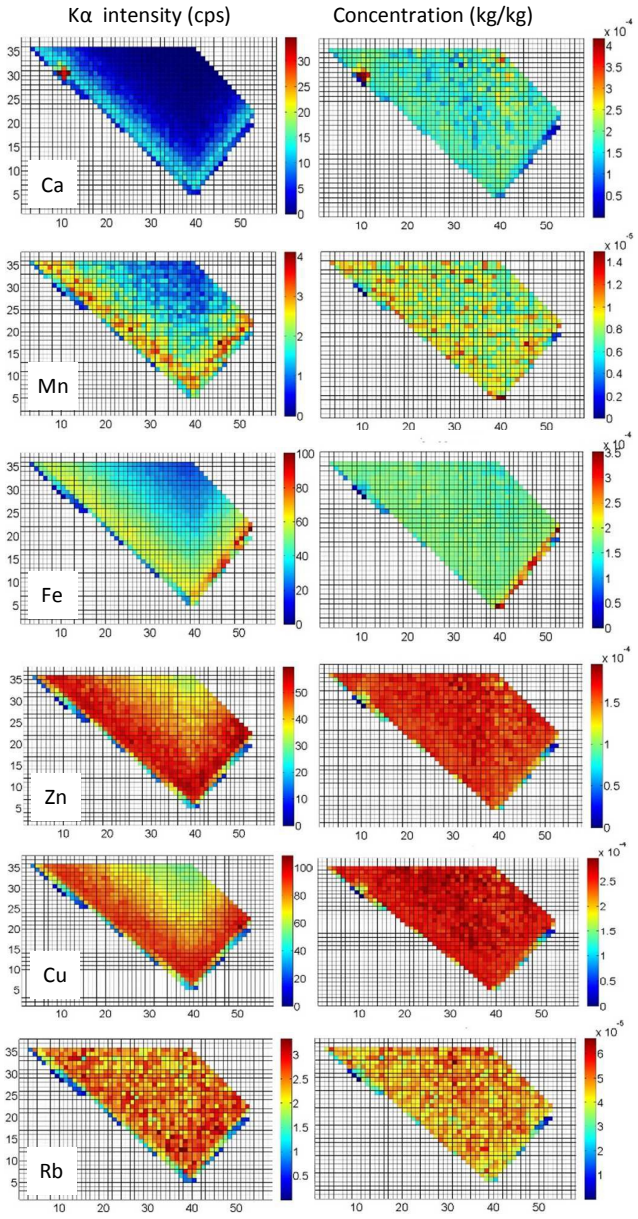

Figure 7. Intensity distribution of Kα lines of Ca, Mn, Fe, Cu, Zn and Rb elements (left) and the concentration map (right) calculated by the confocal FPM model on standard reference material NIST SRM 1577c. Energy of the excitation beam was 19.5 keV.

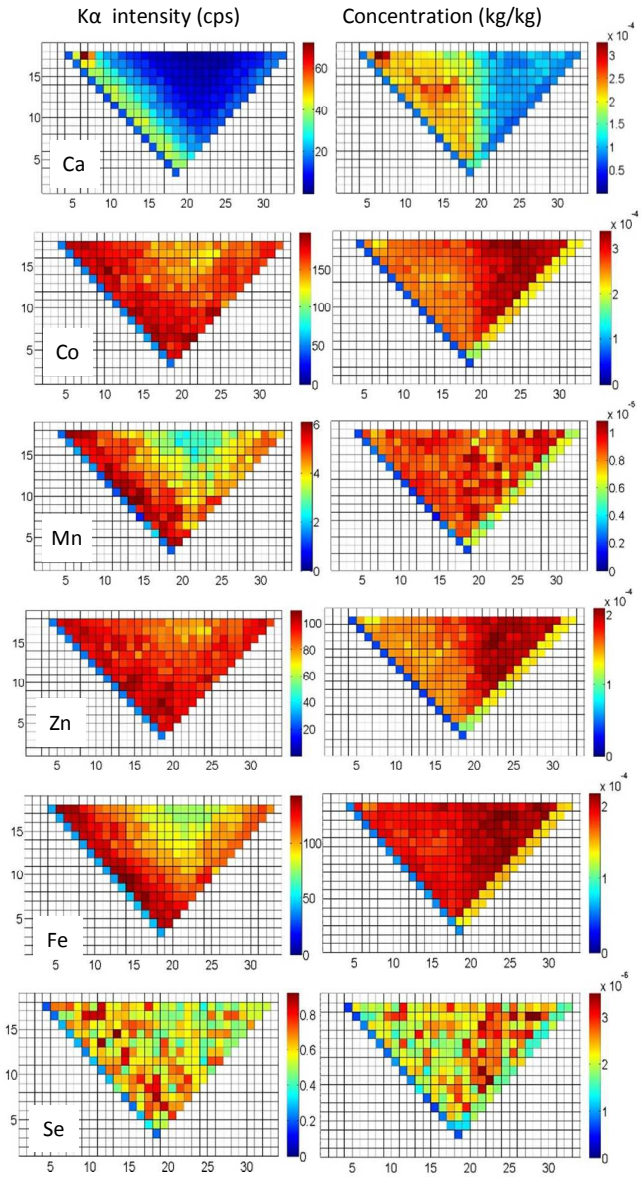

Figure 8. Intensity distribution of Kα lines of Ca, Mn, Fe, Co, Zn and Se elements (left side) and the concentration map (right side) of these elements calculated by recent model of confocal FPM on standard reference material NIST SRM 1577c. Energy of the excitation beam was 17.0 keV.

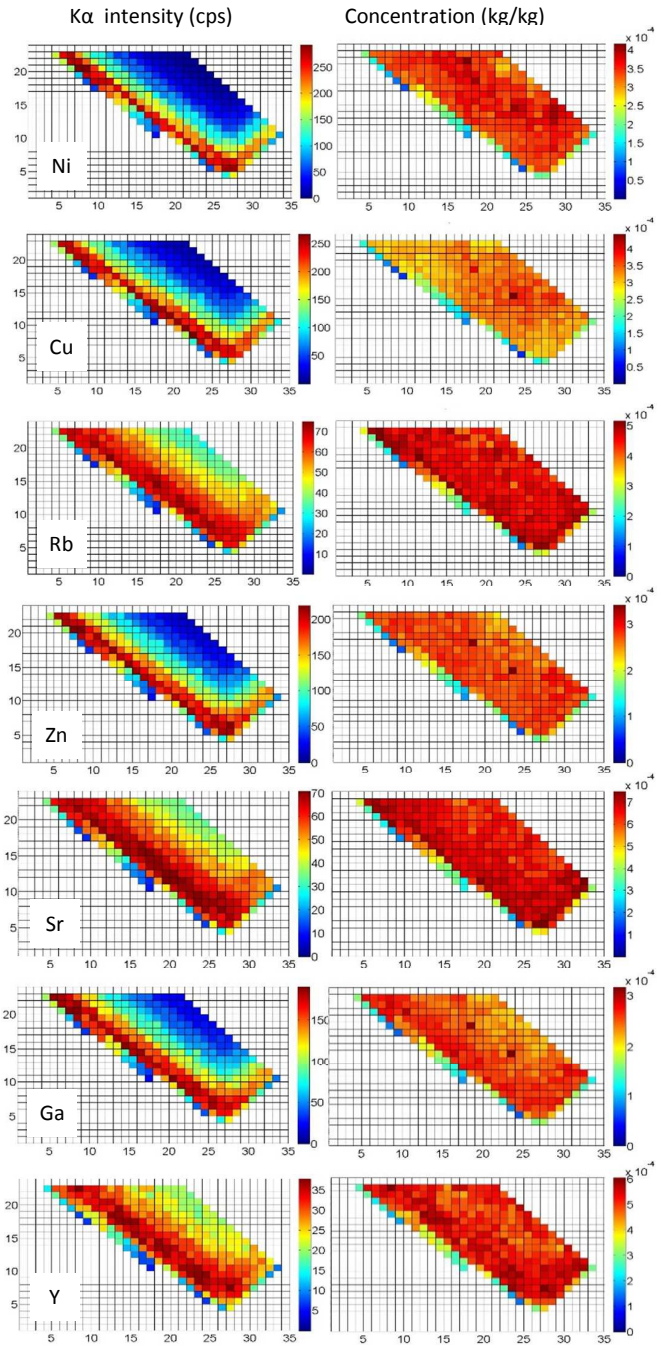

Figure 9. Results of the confocal measurement and FPM calculation: Kα intensity distribution (left) and map of concentrations (right) on standard glass reference material (NIST SRM-611) for elements Co, Ni, Cu, Zn, Ga, Rb, Sr, Y, Zr. The energy of the excitation SR was 19.5 keV. The pixel area of the beam was 20x20 μm^2 and the measuring time was set as 40 sec for each pixel.

For comparison of the calculated and nominal concentrations, we determined the average concentrations of the analysed volume of the sample. The limit for the maximum depth for quantification depends on the uncertainty of the calculated concentrations in individual voxels estimated by the error of the characteristic intensities. Table 2. contains the comparison of the calculated average and the certified nominal concentrations[39]. The error of the calculated concentrations depends on different factors such as statistic of the detected counts, or the uncertainty of the parameters used for FPM calculations. Increasingly with the depth from where the secondary X-rays are emitted the detected intensities decrease. This should result that the dominant source of the uncertainty of the detected X-ray fluorescence intensities is statistical. This effect generates a depth-limit for applicability of the recent numerical calculations.

Element	Nominal concentration (mg/kg)	Average value of FPM calculated concentration (mg/kg) E=17 keV	Average value of FPM calculated concentration (mg/kg) E=19.5 keV
Ca	131 ± 10	153 ± 52	182 ± 57
Mn	10.46 ± 0.47	8.4 ± 2.2	8.3 ± 3.4
Fe	198 ± 0.65	194 ± 18	170 ± 20
Cu	275.2 ± 4.6	293 ± 27	257 ± 23
Zn	181.1 ± 1.0	180 ± 19	163 ± 16
Rb	35.3 ± 1.1	----	46.8 ± 9.5

Table 2. Nominal and FPM calculated concentrations of NIST SRM-1577c Bovine liver standard sample measured at SR energy of 17 keV and 19.5 keV.

Conclusions

A new quantitative reconstruction procedure and a specialised numerical algorithm for solution of the mathematical model have been developed for X-ray fluorescence confocal imaging. The theoretical model and the algorithm of the solution were validated by μXRF analysis of standard biological and glass samples using monochromatic synchrotron radiation at HASYLAB Beamline L. The mathematical description of the theoretical model is based on a new version of Fundamental Parameter Method that allows approaching 2D or 3D maps of the concentration values of the sample elements in depth. The main difficulty of the reconstruction procedure in the 2D quantitative μXRF calculation is the simultaneous solution of huge number of non-linear equations describing the relationship between the weight fractions of elements and their X-ray fluorescence intensity. We have developed a new iterative procedure based on numerical successive approximation of sample composition in each individual voxel that method provides a possibility to avoid the serious numerical difficulty in the simultaneous solution of FPM equations. New finding in this research was the development of a new optimized numerical procedure offering a separated solution of the FPM model for all voxels in the sample. The order of calculation steps follows geometrically the path of primary and secondary X-ray beams and in each step of calculations, performed voxel-by-voxel, utilizes the results of the calculated compositions performed in the previous voxels. The current FPM model considers the absorption of heterogeneous composition of the sample for both primary and secondary X-ray beams and calculates the photoelectric excitation process in each voxel. The limit of validation of the method in depth of the sample body depends on the absorption properties of the matrix; for biological samples the analysed depth is about 50-300 μm depending on the atomic number of the analysed elements. This new FPM model and the numerical procedure for solution were successfully tested on biological and glass samples using synchrotron radiation. The possible main field of application of this recently developed new algorithm is perhaps the investigation of light matrix samples especially biological materials in which the major components are low-Z elements (Z<10) and the analytical task is to determine the minor and trace elements.

Acknowledgement

This work has been partly carried out in the frame of VKSZ-14-1-2015-0021 Hungarian project supported by the National Research, Development and Innovation Found.

1 U. E. A. Fittschen, G. Falkenberg, Anal. Bioanal. Chem., 2011, 400,1743.
2 L. Vincze, B. Vekemans, F. E. Brenker, G. Falkenberg, K. Rickers, A. Somogyi, M. Kersten, F. Adams, Anal. Chem., 2004, 76, 6786.
3 K. Proost, L. Vincze, K. Janssens, N. Gao, E. Bulska, M. Schreiner and G. Falkenberg, X-Ray Spectrom., 2003, 32, 215.
4 R. Padilla, P. Van Espen, A. Abrahantes, K. Janssens, X-Ray Spectrom., 2005, 34: 19–27.
5 V. D. Hodoroaba, M. Procop, X-Ray Spectrom., 2009, 38, 216.
6 W. Malzer, B. Kanngieher, Spectrochim, Acta B, 2005, 60, 1334.
7 Z. Smit, K. Janssens, K. Proost, I. Langus, Nucl. Instrum. Meth. B, 2004, 219–220, 35.
8 I. Schaumann,W. Malzer, I. Mantouvalou, L. Lühl, B. Kanngießer, R. Dargel, U. Giese, C. Vogt, Spectrochim. Acta B, 2009, 64, 334.
9 A.R. Woll, J. Mass, C. Bisulca, R. Huang, D. H. Bilderback, S. Gruner, N. Gao, Appl. Phys. A, 2006, 83, 235.
10 R. D. Perez, H. J. Sanchez, M. Rubio, C. A. Perez, X-Ray Spectrom., 2011, 40, 19.
11 D. Sokaras, A. G. Karydas, Anal. Chem., 2009, 81, 4946.

12 T. Wolff, W. Malzer, I. Mantouvalou, O. Hahn, B. Kanngießer, Spectrochim. Acta B, 2011, 66, 170.
13 M.R. Gherase, D.E.B. Fleming, Nucl. Instrum. Meth. B, 2011, 269, 1150.
14 K. Tsuji, K. Nakano, J. Anal. At. Spectrom., 26, 305–309, 2011.
15 L. Xiaoyan, W. Zhihong, S. Tianxi, P. Qiuli, D. Xunliang, Nucl. Instrum. Meth. B, 2008, 266, 2638.
16 T. Yonehara, D. Orita, K. Nakano, S. Komatani, S. Ohzawa, A. Bando, H. Uchihara, K. Tsuji, X-Ray Spectrom., 2010, 39, 78.
17 B. Kanngießer, W. Malzer, A. F. Rodriguez, I. Reiche, Spectrochim. Acta B, 2005, 60, 41.
18 B. Kanngießer, W. Malzer, I. Reiche, Nucl. Instrum. Meth. B, 2003, 211, 259.
19 I. Mantouvalou, K. Lange, T. Wolff, D. Grötzsch, L. Lühl, M. Haschke, O. Hahnb, B. Kanngießer, J. Anal. At. Spectrom., 2010, 25, 554.
20 J. Dik, K. Janssens, G. Van Der Snickt, L. van der Loeff, K. Rickers, M. Cotte, Anal. Chem., 2008, 80, 6436.
21 B. Kanngießer, W. Malzer, M. Pagels, L. Lühl, G. Weseloh, Anal. Bioanal. Chem., 2007, 389, 1171.
22 V. G. Mihucz, G. Silversmit, I. Szalóki, B. Samber, T. Schoonjans, E. Tatár, L. Vincze, I. Virág, J. Yao, Gy. Záray, Food Chem., 2010, 121,290.
23 B. De Samber, G. Silversmit, K. De Schamphelaere, R. Evens, T. Schoonjans, B. Vekemans, C. Janssen, B. Masschaele, L. Van Hoorebeke, I. Szalóki, F. Vanhaecke, K. Rickers, G. Falkenberg and L. Vincze, J. Anal. Atom. Spectrom., 2010, 25, 544.
24 S. Schmitz, F. E. Brenker, T. Schoonjans, B. Vekemans, G. Silversmit, L. Vincze, M. Burghammer, C. Riekel, Geochim. Cosmochim. Ac., 2009, 73, 5483.
25 Brenker FE, Vollmer C, Vincze L, Vekemans B, Szymanski A, Janssens K, Szaloki I, Nasdala L, Joswig W, Kaminsky F, Earth Planet. Sc. Lett., 2007, 260, 1-9.
26 K. Janssens, W. De Nolf, G. Van Der Snickt, L. Vincze, B. Vekemans, R. Terzano, F. E. Brenker, Trends in Analytical Chemistry, 2010, 6, 29.
27 C. A. MacDonald, X-Ray Optics and Instrum., 2010, Article ID 867049.
28 I. Szalóki, A. Somogyi, M. Braun, A. Tóth, X-Ray Spectrom. 28, 399-405, 1999.
29 M. Haschke, M. Haller, X-Ray Spectrom., 32, 239–247, 2003.
30 K. Proost, L. Vincze, K. Janssens, N. Gao, E. Bulska, M.Schreiner, G. Falkenberg, X-Ray Spectrom., 32, 215–222, 2003.
31 J. Xie, Y. Yan, X. Ding, Y. He, Q. Pan, X-Ray Spectrom., 29, 305–309, 2000.
32 I. Szalóki , S. Szegedi, K. Varga, M. Braun, J. Osán, R. Van Grieken, X-Ray Spectrom., 30, 49-55, 2001.
33 D. Wegrzynek, A. Markowicz, E. Chinea-Cano, X-Ray Spectrom., 32: 119–128, 2003.
34 I. Mantouvalou, W. Malzer, I. Schaumann, L. Lühl, R. Dargel, C. Vogt, B. Kanngiesser, Anal. Chem., Vol. 80, pp. 819-826, 2008.
35 D. Gupta, J.M. Chatterjee, R. Ghosh, A. K.Mitra, S. Roya, M. Sarkara, X-Ray Spectrom., 39, 6, 364-371, 2010.
36 I. Szalóki, X-Ray Spectrom., 20, 297-305, 1991.
37 B. Vekemans, K. Janssens, L. Vincze, F. Adams, P. Van Espen, X-Ray Spectrom., Vol. 23, pp. 278–285, 1994.
38 S. A. Wise, R. L. Watters, Certificate of Analysis, Standard Reference Material 1577c, Bovine Liver, National Institute of Standards & Technology, Gaithersburg, MD 20899, 2009.
39 S. A. Wise, R. L. Watters, Certificate of Analysis, Standard Reference Material 611, Trace Elements in Glass Matrix, National Institute of Standards & Technology, Gaithersburg, MD 20899, 2012.